

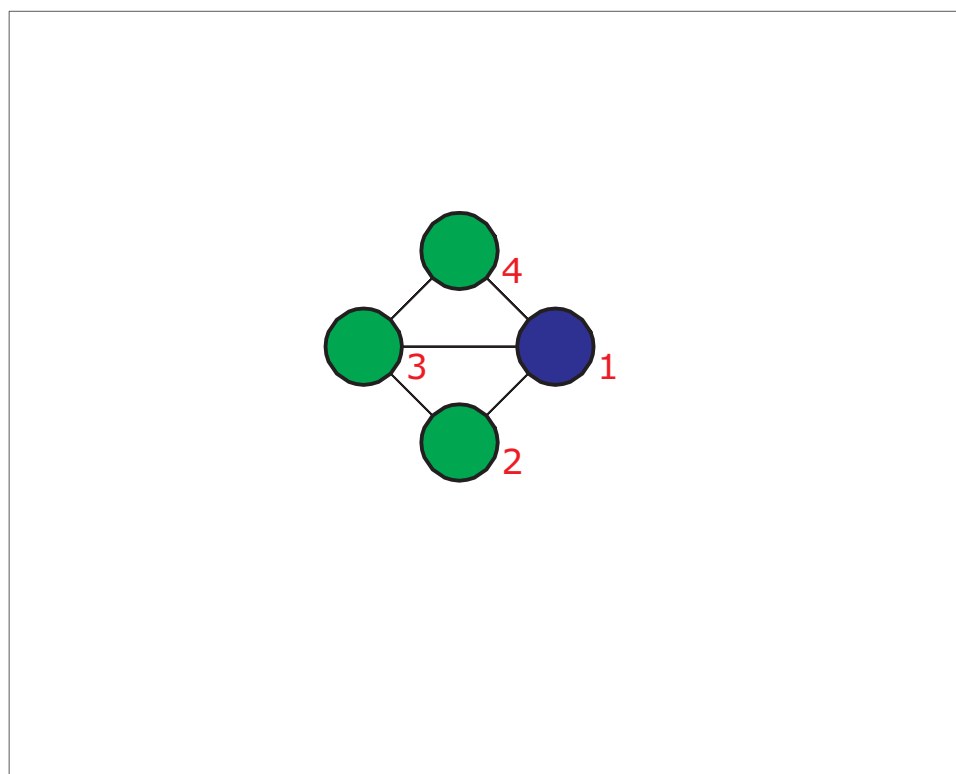
Supporting Information for

A state-mutating genetic algorithm to design ion channel models

by V. Menon, N. Spruston and W. L. Kath

Northwestern University

This document contains additional information that accompanies the main paper. Supporting videos, figures, tables and text are included in the order in which they are referenced in the main paper.



Supporting Video 1: This video shows the best topologies at various generations throughout the running of the genetic algorithm. In all topologies, the blue state is the open state. The locations of the states do not have any specific meaning; they are moved as the topology changes merely to prevent excessive edge crossings in the state diagram. For ease of viewing, the open state position was kept fixed. This movie was created using SoNIA (Social Network Image Animator, www.stanford.edu/group/sonia/).

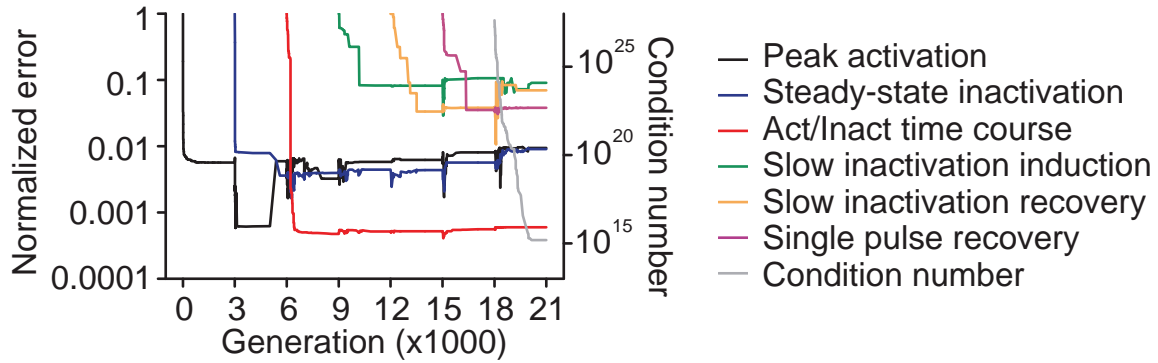


Figure S1: Plot of genetic algorithm error as a function of generation number. The error for each protocol is normalized to the initial error calculated at the beginning of the optimization process for that protocol. The condition number is the ratio of the largest to the smallest time scale in the model.

Table S1: Rate parameters for a 6-state model exhibiting slow inactivation, obtained from a duplicate run of the genetic algorithm. The topology of this model is the same as the optimal model described in the main text. Rate constants are in the form $r_{ij} = \exp(a + bV)$, where r_{ij} is the rate from state j to state i .

r_{ij}	a	b	r_{ij}	a	b
r_{31}	5.018	0.1066	r_{13}	-5.018	-0.1773
r_{32}	2.186	0.04433	r_{23}	-2.186	-0.1498
r_{52}	5.230	0.2300	r_{25}	-5.085	-0.04757
r_{43}	-21.27	-0.2987	r_{34}	-6.939	0.006088
r_{63}	0.5123	0.005261	r_{36}	14.85	0.2956
r_{54}	-12.07	-0.3327	r_{45}	-32.35	-0.4215
r_{65}	-3.671	0.04366	r_{34}	16.61	0.4175

Table S2: Rate parameters for a 6-state model exhibiting slow inactivation, obtained from a duplicate run of the genetic algorithm. The topology of this model has the same number of states as the optimal model described in the main text, but has one extra edge. Rate constants are in the form $r_{ij} = \exp(a + bV)$, where r_{ij} is the rate from state j to state i .

r_{ij}	a	b	r_{ij}	a	b
r_{31}	4.963	0.03196	r_{13}	-4.963	-0.2482
r_{32}	2.102	0.05011	r_{23}	-2.102	-0.1446
r_{21}	-2.646	-0.04348	r_{12}	3.076	0.04194
r_{52}	5.507	0.2415	r_{25}	-4.962	-0.03840
r_{43}	-32.09	-0.4343	r_{34}	-17.75	-0.1512
r_{63}	0.5520	0.005470	r_{36}	14.89	0.2959
r_{54}	-14.70	-0.09322	r_{45}	-35.30	-0.4615
r_{65}	0.3515	0.4194	r_{56}	20.95	0.7950

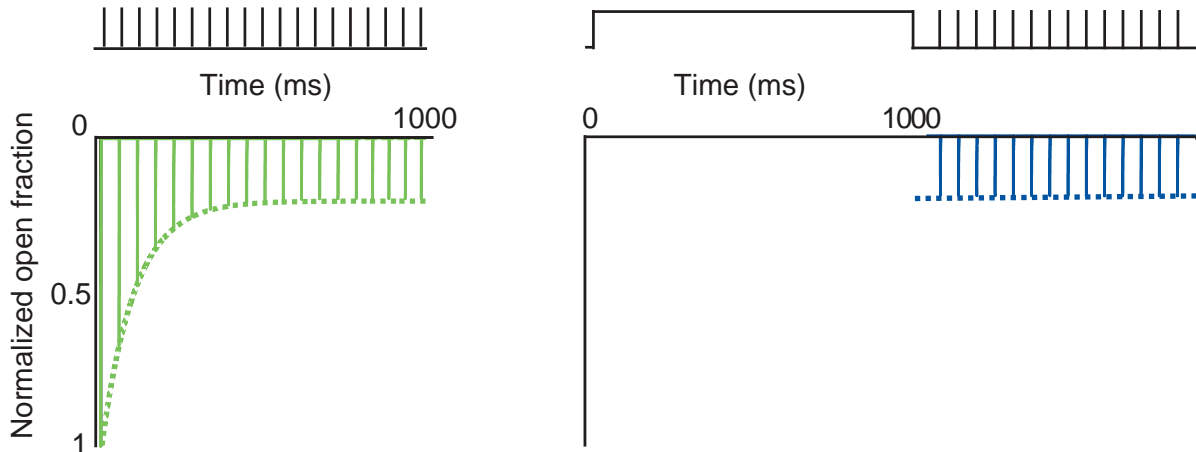


Figure S2: Behavior of the optimal 6-state model under a protocol not used in the fitting procedure. For this model, prolonged inactivation induced by a train of depolarizing pulses (right) is indistinguishable from inactivation induced by sustained depolarization (left). Dashed lines represent experimentally-observed prolonged inactivation. See text for additional discussion.

Table S3: Rate parameters for 5-state model with no slow inactivation. Rate constants are in the form $r_{ij} = \exp(a + bV)$, where r_{ij} is the rate from state j to state i .

r_{ij}	a	b	r_{ij}	a	b
r_{31}	5.218	0.1066	r_{13}	-5.018	-0.1772
r_{32}	2.147	0.04433	r_{23}	-2.780	-0.1498
r_{52}	5.498	0.2200	r_{25}	-5.371	-0.05757
r_{43}	0.5124	0.004891	r_{34}	14.85	0.2960
r_{54}	16.61	0.4407	r_{45}	-3.671	0.06612

Table S4: Rate parameters for a 14-state model exhibiting slow inactivation. The topology of this model was modified from a previous 12-state sodium channel model [1], as shown in Supplemental Figure S3A. Rate constants are in the form $r_{i,j} = \exp(a + bV)$, where $r_{i,j}$ is the rate from state j to state i .

$r_{i,j}$	a	b	$r_{i,j}$	a	b
$r_{2,1}$	-1.397	-0.003761	$r_{1,2}$	-1.5936	0.003761
$r_{3,2}$	2.586	0.002927	$r_{2,3}$	2.783	-0.002927
$r_{4,3}$	-0.1228	-0.02137	$r_{3,4}$	-0.1228	0.02137
$r_{5,4}$	5.148	0.07770	$r_{4,5}$	5.148	-0.07770
$r_{6,5}$	7.477	0.06274	$r_{5,6}$	-7.477	-0.06274
$r_{7,1}$	0.0000	0.0000	$r_{1,7}$	0.0000	0.0000
$r_{8,2}$	-0.003030	-0.03661	$r_{2,8}$	0.003030	-0.04414
$r_{9,3}$	2.356	0.01530	$r_{3,9}$	-2.347	-0.01530
$r_{10,4}$	0.003885	-0.009197	$r_{4,10}$	-0.01803	-0.05146
$r_{11,5}$	-0.9504	-0.1504	$r_{5,11}$	3.239	-0.03936
$r_{12,6}$	0.4384	0.01225	$r_{6,12}$	-3.388	-0.01237
$r_{8,7}$	0.09541	0.0000	$r_{7,8}$	-0.09541	0.0000
$r_{9,8}$	2.256	0.01447	$r_{8,9}$	-2.256	-0.01447
$r_{10,9}$	-2.341	-0.01554	$r_{9,10}$	2.341	0.01554
$r_{11,10}$	-2.111	0.001071	$r_{10,11}$	2.111	-0.001071
$r_{12,11}$	11.49	0.2437	$r_{11,12}$	-11.49	-0.01733
$r_{13,5}$	-20.17	-0.05550	$r_{5,13}$	20.17	0.05550
$r_{14,6}$	-14.56	-0.1719	$r_{6,14}$	-1.124	0.06450
$r_{14,13}$	20.93	0.0000	$r_{13,14}$	-20.93	0.0000

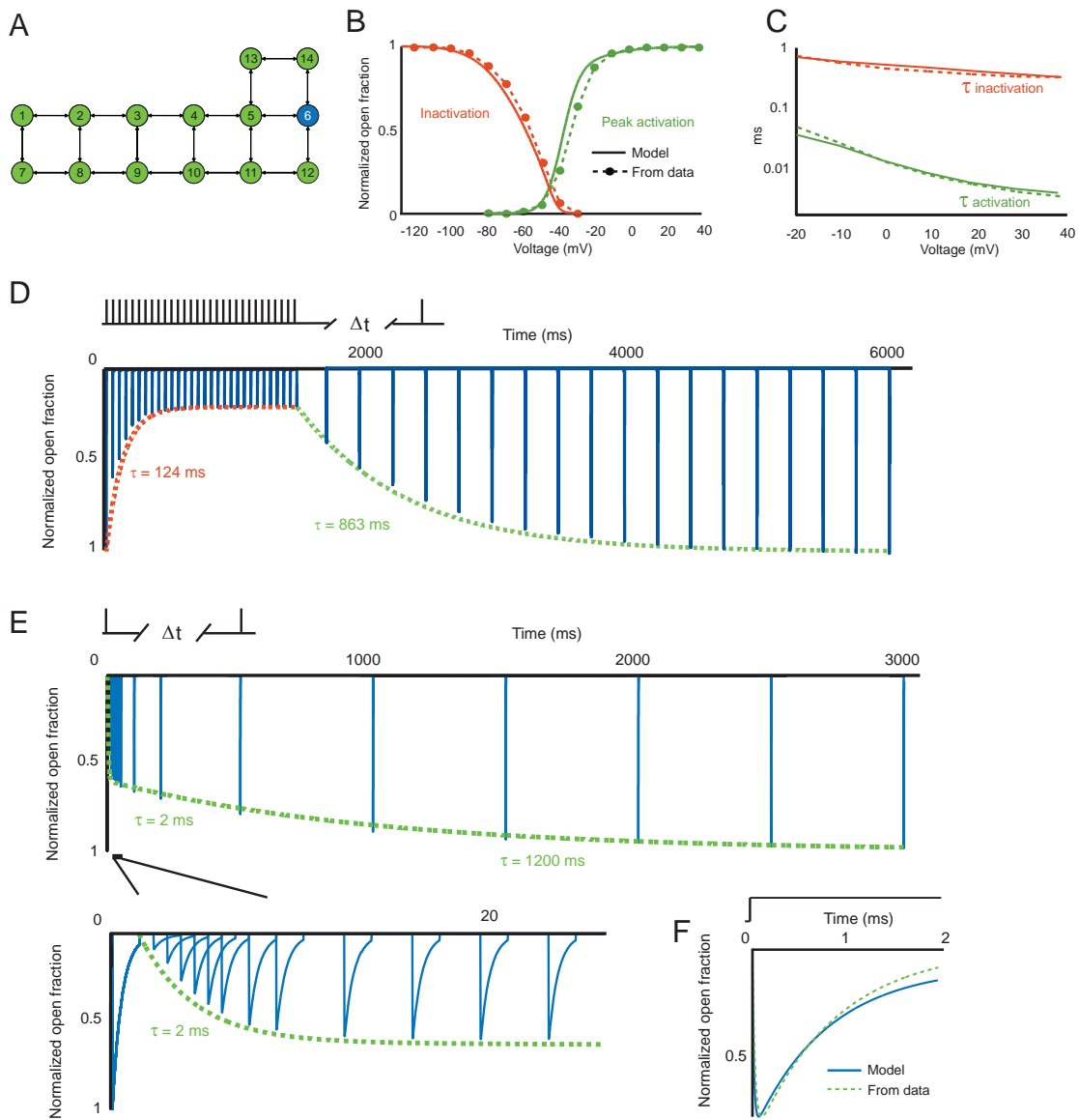


Figure S3: Summary of voltage clamp simulation behavior for a 14-state model. The rate parameters of this model were optimized using the genetic algorithm, while fixing the topology, which is a modified version of a 12-state model postulated by Kuo and Bean. A. Topology of the 14-state model. The blue state (state 6) corresponds to the open conductance state. B. Voltage-dependent activation and inactivation curves for the model (solid lines) and from experiments (dashed lines). C. Activation and inactivation time constant curves for the model (solid lines) and from experiments (dashed lines). D. Entry into and recovery from prolonged inactivation induced by a train of 20 Hz pulses. As per voltage clamp convention, the negative of the open fraction is plotted on the y-axis. The first 1000 ms shows the decline in peak open fraction resulting from the 20 Hz train of depolarizing pulses. The remaining points represent the peak open fraction during depolarizing test pulses delivered at various intervals. E. Two-phase recovery from inactivation induced by a single depolarizing pulse. The model exhibits a bi-exponential time course of recovery, with two distinct phases. The lower panel is a close-up of the first 20 ms, showing the initial phase of the two-phase recovery from a single pulse. F. Model response (solid line) to a single step depolarization from -70 mV to -1 mV, showing agreement with experimentally observed time course of activation and inactivation (dashed line).

List of fitting protocols

Below are detailed descriptions of the fitting protocols used in the genetic algorithm.

1. Peak activation: This protocol consists of holding at -120 mV and then stepping to the test voltage (ranging from -80 mV to 40 mV in 10 mV intervals) for 30ms and measuring the peak open fraction. The protocol and experimental data were obtained from [2], Figure 1C.
2. Steady-state inactivation: This protocol consists of holding at -90 mV, stepping to the test voltage (ranging from -120 mV to -30 mV in 10 mV intervals) for 50 ms, and then stepping up to 0 mV for 30 ms and measuring the peak open fraction. The protocol and experimental data were obtained from [2], Figure 3C.
3. Activation and fast inactivation time course: This protocol consists of holding at -66 mV, and then stepping up to the test voltage (ranging from -21 mV to 39 mV in 10 mV intervals) for 5 ms, and comparing the resulting trace to that generated using the experimentally-obtained time constants of activation and fast inactivation in the exponential form $V(t) = (1 - e^{-t/\tau_{act}})e^{-t/\tau_{inact}}$. The protocol and experimental data were obtained from [3], Figures 3 and 4. Note that referenced data were presented both at 12 °C and 23 °C, and the voltage-dependent activation and inactivation time constant curves at 23 °C were found to have the same shape as the 12 °C data if they were divided by constants — 2.8 for activation and 2.4 for inactivation. To scale the data up to 34 °C, a temperature more appropriate for the other fitting data used here, the voltage-dependent activation and inactivation curves were therefore divided by these constants again. The factor 2.8 is close to the expected temperature-dependent scaling [4].
4. Entry into slow inactivation induced by a train of 20 Hz pulses: This protocol consists of holding at -71 mV, followed by a series of 2 ms-wide 50 mV amplitude depolarizing pulses at 20 Hz for 1 second with interspike voltage equal to -71 mV. The peak open fraction is measured during each 2 ms depolarizing pulse. The protocol and experimental data were obtained from [5], which show an exponential time course for entry into the slow inactivated state with $\tau=124$ ms.
5. Recovery from slow inactivation induced by a train of 20 Hz pulses: After inducing entry into slow inactivation using the protocol described above, this protocol consists of holding at -71 mV for a variable interval (ranging from 100 ms to 4200 ms in 100 ms intervals) to allow for recovery, and then measuring the peak open fraction during a 2ms wide, 50 mV amplitude depolarizing test pulse. The protocol and experimental data were obtained from [5], Figure 2, which shows an exponential time course for recovery with $\tau=863$ ms.
6. Two-phase recovery from inactivation induced by a single pulse: This protocol consists of holding at -71 mV, followed by a single 2 ms-wide 70 mV amplitude depolarizing pulse, then a variable recovery interval (comprising 2 ms, 3 ms, 4 ms, 5 ms, 10 ms, 20 ms, 100

ms, 200 ms, 500 ms, 1000 ms, 1500 ms, 2000 ms, or 2500 ms) at -71 mV, and finally measuring the peak open fraction during a 2 ms-wide 70 mV amplitude depolarizing test pulse. The protocol and experimental data were obtained from [5], Figure 6B, which shows a bi-phasic recovery with a fast time constant of 2 ms and a slow time constant of 1200 ms.

7. Q matrix condition number: In order to avoid generating models with excessively stiff Q matrices, an additional protocol was added to minimize the condition number of the rate matrix Q over the physically relevant voltage range of operation (-100mV to 40mV). The condition number was defined as the logarithm of the ratio of the largest and smallest magnitude non-zero eigenvalues; these eigenvalues are related to the fastest and slowest time constants associated with the transitions in the model. This minimizes numerical difficulties associated with solving the differential equations for the time evolution of the states.

Table S5: Rate parameters for a 6-state model exhibiting slow inactivation, with piecewise linear-exponential functions. Rate constants are in the form $r_{ij} = \exp(a + bV)$, where r_{ij} is the rate from state j to state i . There are two values for each constant b , one for $V > 0$ and one for $V < 0$.

r_{ij}	a	$b(V < 0)$	$b(V > 0)$	r_{ij}	a	$b(V < 0)$	$b(V > 0)$
r_{31}	5.218	0.1066	-0.01622	r_{13}	-5.018	-0.1772	0.02036
r_{32}	2.187	0.04433	-0.001762	r_{23}	-2.819	-0.1498	0.03441
r_{52}	6.863	0.2200	-0.02776	r_{25}	-4.085	-0.05757	0.02071
r_{43}	-11.53	0.03047	-0.01214	r_{34}	-18.68	-0.000002500	0.01290
r_{63}	0.5124	0.005264	0.01877	r_{36}	14.85	0.2956	-0.01877
r_{54}	-2.802	0.05300	0.006364	r_{45}	-1.599	0.0000	-0.006386
r_{65}	-3.671	0.04366	-0.001354	r_{56}	16.61	0.4175	-0.05119

Compartmental models

In the multi-compartmental simulations carried out using NEURON [6], two types of sodium conductance were used: the optimal channel model exhibiting prolonged inactivation, and the model with only fast recovery from inactivation obtained by eliminating the prolonged inactivation state and re-optimizing the rate parameters. The total sodium conductance in the apical and basal dendrites was 0.05 S/cm^2 and 0.03 S/cm^2 , respectively, and the amount of slowly inactivating sodium as a proportion of total sodium conductance varied from 0% at the soma to 100% in distal dendrites, reflecting the experimentally observed gradient of sodium channels exhibiting prolonged inactivation [5]. The other conductances were chosen to replicate those from a previous simulation [7], and included a non-uniform leak conductance, a delayed rectifier K^+ conductance [8], an A-type K^+ conductance with proximal and distal versions [9, 10], and an I_h conductance [11]. Additional details associated with the compartmental models are provided in Table S6.

Table S6: Passive properties and channel conductances in the dendrites of the multi-compartmental model. Here x represents the distance of the dendritic segment from the soma in μm . All conductances are in S/cm^2 .

Property/Conductance type	Value
Axial resistivity	$117.15 \text{ } \Omega\text{cm}$
Membrane capacitance	$1.5657 \text{ } \mu\text{F/cm}^2$
Leak conductance	$(33938 + 248072/(1 + \exp((x - 186.04)/31.681)))^{-1}$
Apical H conductance	$0.03794 + 19.961206/(1 + \exp(-(x - 316.65)/20))$
Basal H conductance	0.03794
Delayed-rectifier K conductance	0.1
A-type conductance	$0.2(1 + 0.007(\min(x, 450)))$
Apical slow-inactivating Na conductance	$(0.05)(\min(0.0025x, 1))$
Apical fast-inactivating-only Na conductance	$(0.05)(1 - (\min(0.0025x, 1)))$
Basal fast-inactivating Na conductance	0.03
Basal slow-inactivating-only Na conductance	0

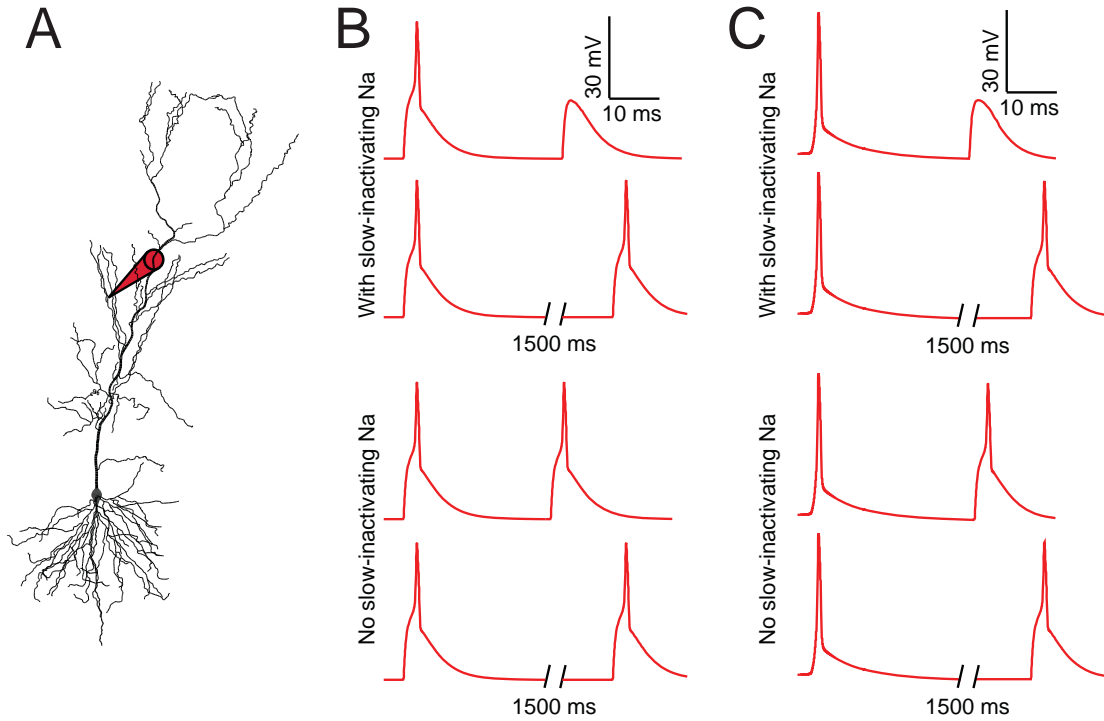


Figure S4: Simulations examining the role of prolonged sodium channel inactivation in the inhibition of dendritic spike generation by prior local depolarization [12,13]. Membrane parameters are given in Table S6. For the branch examined, dendritic spikes were elicited by coincident, localized activation of 5 synapses with a total peak conductance of 2.3 nS and kinetics of the form $i = g_{max}(e^{-t/2} - e^{-t/0.2})(V - 0)$. A backpropagating action potential (bAPs) was generated by a 30 ms, 0.15 nA somatic current injection. A. Shape plot showing the location of the recording electrode. B. Local dendritic spike attenuation: synaptic activation generating a dendritic spike prevents a second synaptic activation from producing a dendritic spike in the same branch 30 ms later (top trace). After a delay of 1000 ms, however, a second dendritic spike can be generated (second trace). This phenomenon is not observed in the absence of sodium channels exhibiting prolonged inactivation (bottom two traces). C. Global dendritic spike attenuation: The arrival of a bAP approximately 30 ms before a dendritic spike-generating synaptic stimulus inhibits the spike (top trace). When the delay between the bAP and the stimulus is 1000 ms, the dendritic spike is generated robustly (second trace). This phenomenon is not observed in the absence of sodium channels exhibiting prolonged inactivation (bottom two traces).

References

- [1] C. C. Kuo and B. P. Bean. Na⁺ channels must deactivate to recover from inactivation. *Neuron*, 12(4):819–829, 1994.
- [2] M. Martina and P. Jonas. Functional differences in Na⁺ channel gating between fast-spiking interneurons and principal neurons of rat hippocampus. *J. Physiol.*, 505:593–603, December 1997.
- [3] G. Baranauskas and M. Martina. Sodium currents activate without a Hodgkin and Huxley-type delay in central mammalian neurons. *J. Neurosci*, 26(2):671–684, 2006.
- [4] Hille B (2001). *Ion channels of excitable membranes* (Sinauer, Sunderland, MA)
- [5] T. Mickus, H. Jung, and N. Spruston. Properties of slow, cumulative sodium channel inactivation in rat hippocampal CA1 pyramidal neurons. *Biophys J*, 76(2):846–860, February 1999.
- [6] Hines ML, Carnevale NT (1997) The NEURON simulation environment. *Neural Computation* 9:1179–1209.
- [7] Golding NL, Mickus TJ, Katz Y, Kath WL, Spruston N (2005) Factors mediating powerful voltage attenuation along CA1 pyramidal neuron dendrites. *J Physiol* 568:69–82.
- [8] Destexhe A, Huguenard J (2001) Which formalism to use for modeling voltage-dependent conductances. In De Schutter E, ed., *Computational Neuroscience: Realistic Modeling for Experimentalists* (CRC Press, Boca Raton, Fla.), pp. 129–158.
- [9] Hoffman DA, Magee JC, Colbert CM, Johnston D (1997) K⁺ channel regulation of signal propagation in dendrites of hippocampal pyramidal neurons. *Nature* 387:869–875.
- [10] Johnston D, *et al.* (2000) Dendritic potassium channels in hippocampal pyramidal neurons. *J Physiol* 525:75–81.
- [11] Stuart G, Spruston N (1998) Determinants of voltage attenuation in neocortical pyramidal neuron dendrites. *J Neurosci* 18:3501–3510.
- [12] Golding NL, Spruston N (1998) Dendritic spikes are variable triggers of axonal action potentials in hippocampal CA1 pyramidal neurons. *Neuron* 21:1189–1200.
- [13] Remy S, Csicsvari J, Beck H (2009) Activity-dependent control of neuronal output by local and global dendritic spike attenuation. *Neuron* 61:906–916.